

Spatial Variability in Soils: High Resolution Assessment with Electrical Needle Probe

Gye Chun Cho¹; Jong-Sub Lee²; and J. Carlos Santamarina³

Abstract: The global response of a soil is affected by spatial as well as temporal scales. An electrical needle-size probe is developed to effectively assess one-dimensional spatial variability. The probe is designed for laboratory specimens (needle diameter 1.2–2.2 mm), and it can be scaled for field applications. Design considerations include the tip shape, insertion disturbance, electrochemical effects, corrosion, operating frequency, and electrical resonance. Two calibration methods are presented to determine local soil permittivity and resistivity from the measured complex impedance; the simplified calibration procedure is based on resistance measurements only. The local electrical parameters permit one to infer the soil porosity and the electrolyte conductivity. The attainable spatial resolution depends on the needle diameter; submillimetric resolution is typically achieved in laboratory applications. Reconstituted sand specimens and undisturbed clayey specimens are tested to explore the resolution potential of this probe. The electrical needle probe clearly detects the spatial variability that results from different specimen preparation methods in sands and soil layering from natural formation histories such as those in varved clays.

DOI: 10.1061/(ASCE)1090-0241(2004)130:8(843)

CE Database subject headings: Corrosion; Electrical resistivity; Interfaces; Layered soils; Porosity; Penetration; Penetrometers.

Introduction

The spatial variability of soil parameters affects macroscale soil response. The effects of spatial variability on soil behavior have been studied in the context of geoprocesses such as soil liquefaction (Popescu and Prevost 1996; Popescu et al. 1997; Kokusho 1999), slope instability (Yong et al. 1977; Tonon et al. 2000), seepage (Griffiths and Fenton 1993; Fenton and Griffiths 1996), and settlement (Paice et al. 1996). The inherent variability of soil properties in natural soil deposits can be very large; the scale of in situ fluctuation or correlation distance has been investigated for different formations (Phoon and Kulhawy 1999).

Spatial variability has an important effect even in relatively small laboratory specimens. Today, the influence of specimen preparation methods on the behavior of soils at intermediate strains is well documented: specimens prepared by the moist tamping method show 200–300% higher cyclical strength than specimens prepared by the dry deposition method (Ladd 1977; Mulilis et al. 1977; Townsend 1978; Ishihara 1993); specimens prepared by the moist vibration method exhibit 250% higher quasisteady state strength than specimens prepared by the dry pluviation method; and moist tamping renders 200% higher quasisteady

state strength than dry pluviation (Vasquez-Herrera and Dobry 1988; DeGregorio 1990; Marcuson et al. 1990). Unlike compression test results, extension test results show the opposite trend (Miura and Toki 1982).

Pore size distribution and its spatial variability can be evaluated using techniques such as mercury porosimetry, gas adsorption, x-ray scattering (Mulilis et al. 1975; Mitchell et al. 1976), small-angle neutron scattering, computed tomography based on x-ray absorption (Desrues et al. 1996), and imaging techniques using cross sections of impregnated soils (Jang et al. 1999). The mercury porosimetry and gas adsorption techniques are limited to small-size specimens. The x-ray scattering technique, which is an indirect method, requires careful calibration and usually gives qualitative information rather than quantitative information. The computed tomography method requires careful calibration and inversion techniques smooth the contrast in mass density. Imaging techniques using cross sections of impregnated soils are practical in sandy soils, its implementation is destructive and the same specimen cannot be measured both before and after testing.

A simple effective technique is proposed herein to assess the spatial variability of sandy or clayey soil specimens with submillimetric resolution. The technique involves a needle-size probe that is pushed into the soil to permit one to measure the local electromagnetic properties of the medium along its path. The paper starts with a brief review of electromagnetic properties, describes the design and calibration of the probe and demonstrates its capabilities.

Electromagnetic Properties of Soils

Small-perturbation electromagnetic waves propagate through the soil mass without causing any permanent effect. Physical interpretation of these measurements permits one to infer important properties about the soil mass including its porosity, volumetric water content, pore fluid characteristics (e.g., permittivity and

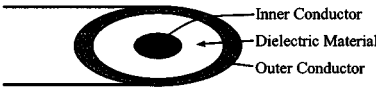
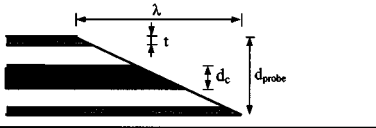
¹Assistant Professor, Civil and Environmental Engineering, KAIST, Daejeon 305-701, Korea.

²Graduate Student, Civil and Environmental Engineering, Georgia Inst. of Technology, Atlanta, GA 30332.

³Professor, Civil and Environmental Engineering, Georgia Inst. of Technology, Atlanta, GA 30332.

Note. Discussion open until January 1, 2005. Separate discussions must be submitted for individual papers. To extend the closing date by one month, a written request must be filed with the ASCE Managing Editor. The manuscript for this paper was submitted for review and possible publication on February 14, 2003; approved on August 13, 2003. This paper is part of the *Journal of Geotechnical and Geoenvironmental Engineering*, Vol. 130, No. 8, August 1, 2004. ©ASCE, ISSN 1090-0241/2004/8-843–850/\$18.00.

Table 1. Characteristics of Needle Probes Used in This Study

Needle Type	Needle Shape			
Side view (0°)				
Side view (90°)				
Needle Number	Needle #1	Needle #2 ^a	Needle #3	Needle #4
Outer Conductor	Stainless S	Stainless S	Stainless S	Copper
Outer Diameter, d_{probe}	2.108mm	2.108mm	1.270mm	2.159mm
Thickness, t	0.254mm	0.254mm	0.216mm	0.241mm
Dielectric Material	Epoxy	Epoxy	Epoxy	PTTF
Inner Conductor	T copper	T copper	T copper	SPCW
Inner Diameter, d_c	0.32mm	0.63mm	0.36mm	0.511mm
Wedge Length, λ	6.10mm	4.50mm	2.72mm	7.20mm
Gap b/w electrode	0.640mm	0.485mm	0.239mm	0.583mm

Note: S=steel; T=tinned; PTTF=polytetrafluoroethylene; SPCW=silver plated copper-weld steel (silver covered copper clad steel).

^aA double wedge tip option is also available.

ionic concentration), fabric anisotropy, and interaction among distinct phases in soils (for a detailed review see Santamarina et al. 2001).

There are three electromagnetic properties. The electrical conductivity σ (or resistivity $\rho=1/\sigma$) is a measure of charge mobility in response to an electric field. Porosity and the conductivity of the electrolyte determine the electrical conductivity.

The complex dielectric permittivity κ^* is frequency dependent, and involves both a real part κ' and an imaginary part κ'' :

$$\kappa^* = \kappa' + j \cdot \kappa'' \quad (1)$$

The real dielectric permittivity κ' represents the polarizability of the material, while the imaginary permittivity captures polarization losses κ''_{pol} . The measured “effective” imaginary permittivity κ''_{eff} combines polarization losses and ohmic conduction σ losses,

$$\kappa''_{eff} = \kappa''_{pol} + \frac{\sigma}{\omega \epsilon_0} \quad (2)$$

where ϵ_0 =permittivity of vacuum ($\epsilon_0=8.85 \times 10^{-12}$ F/m). The complex permittivity reflects the interplay among porosity, volumetric water content, pore fluid characteristics, specific surface, mineralogy, and fabric.

Finally, the complex magnetic permeability μ^* captures the magnetizability and the magnetization losses of the material. Most soils are nonferromagnetic, therefore, the complex permeability μ^* is the permeability of vacuum μ_0 ($\mu^* = \mu_0 = 4\pi \times 10^{-7}$ H/m).

Probe Design

The electrical needle probe is a two-lead coaxial conductor. It is built by inserting an insulated wire (the core electrode) inside a thin metal tube (the external electrode), and filling the annular space with epoxy resin. Then, the tip of the probe is ground and polished to attain the desired tip shape. Prototypes were built with hypodermic needles, stainless steel needles (pipetting needle, Popper and Sons, New York), and semirigid coaxial cables (Pas-

ternack, model PE3678-24). Because the needle probe needs to be mechanically strong to be pushed into the soil, a stainless steel tube is preferred for the outer conductor. Table 1 shows a typical design with a single-wedge tip, and summarizes the geometric characteristics of several similar probes used to gather data in this study.

Probe design and measurement procedures must accommodate not only strength considerations, but electrical, electrochemical, and geometric criteria as well. These are addressed next.

Drainage

Insertion of the needle disturbs the soil. Drainage conditions at the tip depend on the timescale for pore pressure dissipation t_{dis} and the time scale for penetration t_{pen} :

$$\frac{t_{dis}}{t_{pen}} \cong \frac{d^2/c_v}{\lambda/V_{in}} = \left(\frac{d}{\lambda} \right) \frac{dV_{in}}{c_v} \quad (3)$$

where d =diameter of the needle probe; λ is assumed to be the wedge length (Table 1); V_{in} =insertion velocity; and c_v =coefficient of excess pore pressure dissipation. Under undrained penetration conditions, $t_{dis}/t_{pen} \gg 1$, the measurement will not cause local changes in volume. If $t_{dis}/t_{pen} \ll 1$, drained conditions prevail and a change in volume will affect the measured local electrical parameters. Low penetration velocities are used in this study, $V_{in} \approx 1$ cm/min, and drained conditions are anticipated in sands, silts, and low plasticity clays.

Tip Shape

The experience gained with the insertion of penetration probes and piles is relevant to this device as well. However, in this case, the field of volumetric strain around the tip must be analyzed in the context of the zone reached by the electric field that is created at the tip, e.g., based on quasi-DC Laplacian analysis, equivalent to flow net. The following situations can be anticipated:

- A flat tip normal to the needle axis. A dense plug forms and moves with the tip (Vesic 1977). The electric field develops mostly within this plug, therefore a flat tip shape is not recommended.
- A 60° conical tip. The electric field extends within the region that experiences the highest change in volume.
- A sharp, single-wedge tip (see Table 1). Remolding is limited and the field is created along the shortest length, which is in the horizontal direction at the elevation of the core electrode (assuming the needle penetrates vertically). The asymmetric tip may cause the needle to bend in stiff soils.
- A sharp, double-wedge tip. While a change in volume occurs along the wedges, the electric field develops preferentially ahead of the tip, which is where the shortest distance between the core and the external electrode is found; this shape is currently under study at the University of California, Davis (B. Kutter, personal communication).

Soil particles under the tip move down and out. Sharper tips render lesser compression ahead of the penetrometer (Baligh and Scott 1976). The volumetric strain is related with the initial void ratio e and effective confining stress σ' . It can be dilative for low $e-\sigma$ combinations beneath the critical state line, or contractive otherwise. Therefore, if the in situ void ratio is low, a higher void ratio would be measured; but if the in situ void ratio is high, the measured void ratio would be lower. This means that the insertion of a penetration probe tends to homogenize the medium. Volumetric strain at the tip can range from ± 1 to $\pm 4\%$ (Davidson and Boghraat 1983).

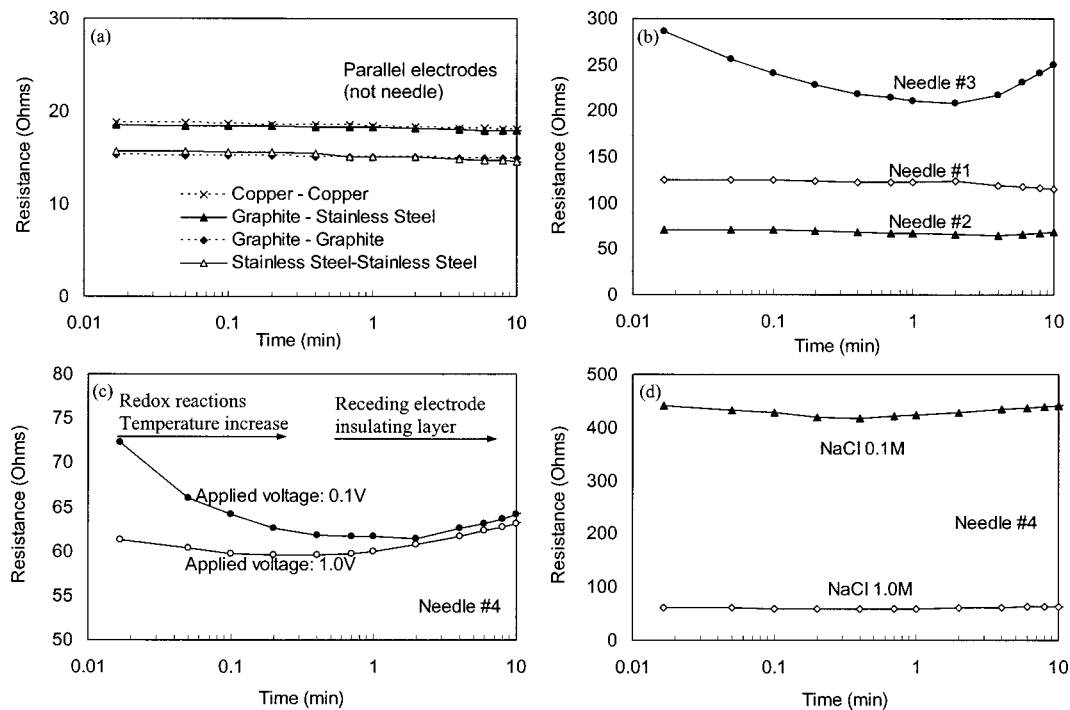


Fig. 1. Corrosion effects over time ($f=100$ kHz, 1 V amplitude, NaCl 1.0 M). Effect of (a) material; (b) geometry; (c) voltage; and (d) electrolyte concentration.

Corrosion

The needle probe forms an electrochemical corrosion cell with the pore fluid: the electrolyte supports ionic conduction, and the external circuit supports electron based conduction. The interface between the two electrical conduction modes is maintained by oxidation at the anode and reduction at the cathode (Bradford 1993).

Redox reactions support electrical continuity between the migrating ions in the electrolyte and the electrons that flow in electrodes and peripheral electronics. As the conductors in the needle probe corrode, the measured electromagnetic parameters change. Corrosion depends on the materials selected for the electrodes, the voltage applied, and the characteristics of the soil and pore fluid. These parameters are studied next (a complete data set can be found in work reported by Lee 2003).

Material

Various potential materials for electrodes were tested under different electrochemical conditions. Tests were run by feeding a continuous AC signal of fixed frequency and amplitude for 10 min (1 V, 100 kHz, 1 M NaCl solution). The spectral impedance response was determined at different stages and compared to that of stable graphite electrodes. Finally, the electrodes tested were inspected using optical microscopy. The evolution in measured resistance for a subset of electrode materials is presented in Fig. 1(a). While stainless steel is selected for the outer conductor on the basis of mechanical strength, its electrochemical performance is not optimal (stainless steel 316 with molybdenum performed better than type 304). On the other hand, copper showed better electrochemical performance and was selected as the material for the core electrode: its central location does not expose the core electrode to significant mechanical demand and copper can sustain the higher corrosion conditions that develop due to the small cross-sectional area of the core conductor.

Effect of Tip Geometry on Corrosion

Three different size needles were used to investigate geometric effects on corrosion (needle Nos. 1, 2, and 3 in Table 1). These needle probes were made of the same material and differed only in the diameter of the electrodes and the wedge angle. The electrolyte was a 1 M NaCl solution, and the signal applied was a 1 V, 100 kHz sinusoid. Typical results are presented in Fig. 1(b). The highest resistance is measured with the smallest needle (needle No. 3) which has the smallest effective area of conductors: as the interelectrode distance decreases, the effective transverse area decreases at a faster rate, hence resistance increases. The resistance measured with needle No. 3 changes significantly over time.

Voltage Effects

Electrode polarization results from incompatible ion-electron flow, and renders the drop in voltage that drives electrode reactions such as oxidation reduction and water dissociation at the electrode-soil interface. Therefore, the voltage applied affects the rate of corrosion. In general, the higher the voltage applied the lower the measured resistance. Voltage-related differences decrease over time as corrosion progresses [Fig. 1(c)]. Several co-existing phenomena are either observed or anticipated: ion liberation and local thermal changes tend to cause the early decrease in measured R values [Fig. 1(c)]. On the other hand, changes in interelectrode distance (out of plane) and the formation of insulating layers of rust causes an increase in measured R values typically observed at later stages [Fig. 1(c)].

Electrolyte Concentration Effects

Electrolyte concentration effects are investigated with needle No. 4 (Table 1) at constant applied frequency (100 kHz) and signal amplitude (1 V). Results in Fig. 1(d) and microscopic observations in Fig. 2 show that as the ionic concentration in the electrolyte increases, the measured resistance decreases, and electrode

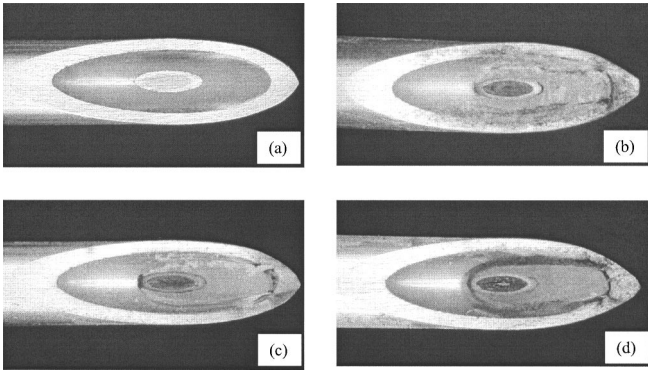


Fig. 2. Corrosion of electrical needle probe after 4 h: (a) before corrosion; (b) self-corrosion by immersion in NaCl 1.0 M with no voltage applied; (c) immersion in NaCl 0.1 M with a 100 kHz, 1 V input signal; and (d) immersion in NaCl 1.0 M with a 100 kHz, 1 V input signal

corrosion increases. The more conductive the electrolyte the lower the drop in voltage within the fluid and the higher the potential difference available at the electrode–fluid interface to drive the redox reactions.

Operating Frequency

The operating frequency range is selected by taking into consideration corrosion effects, electrode polarization, and electrical

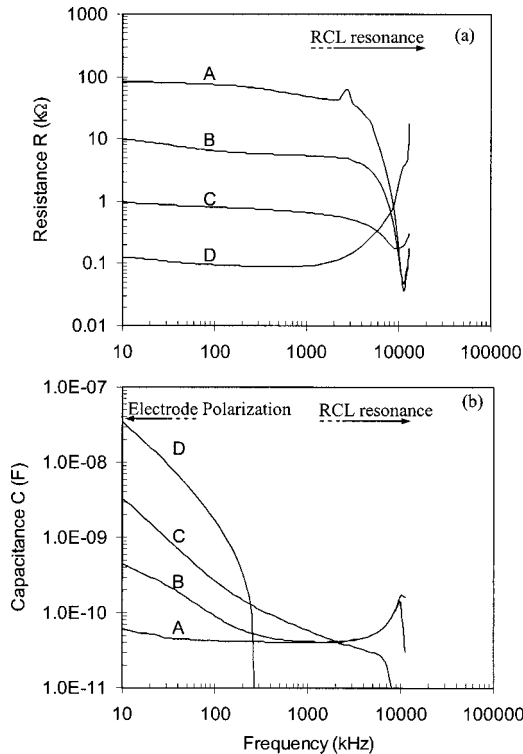


Fig. 3. Resistance and capacitance versus frequency measured in NaCl solutions with different salt concentrations using needle No. 2 (voltage=1 V): (a) Resistance versus frequency; and (b) capacitance versus frequency. The resistivity of the fluids selected is controlled by the salt concentration, i.e., the higher the concentration, the lower the resistivity fluids: (A) 15.6, (B) 2.8, (C) 0.3, and (D) 0.04 kΩ cm.

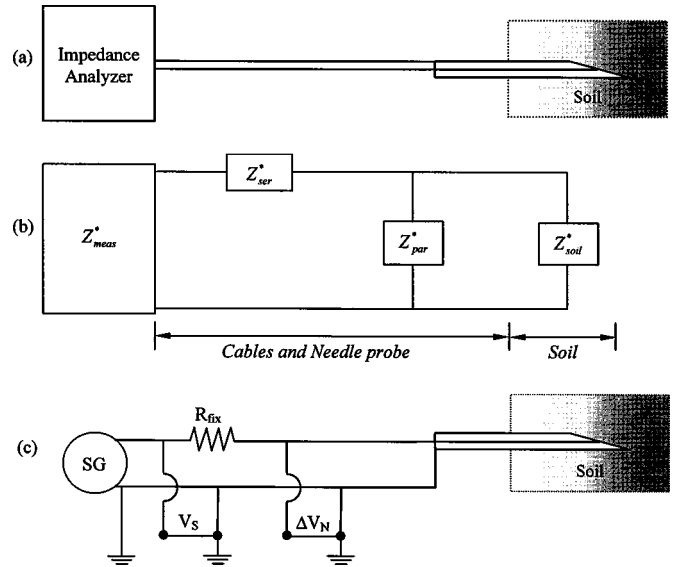


Fig. 4. Circuit analysis for the needle probe: (a) setup; (b) equivalent circuit for the needle probe (asterisks denote complex quantity); (c) simplified measurement procedure (SG: signal generator; V_s : voltage at signal generator; and ΔV_N : voltage drop at needle probe)

resonance in the circuit. Spectral data obtained with different ionic concentration electrolytes are shown in Fig. 3. Resistance R and capacitance C measurements exhibit the effects of electronic resonance at $f > 2$ MHz: this is a typical RCL resonator and the resonant frequency depends on the needle size, cables, and soil–fluid conductivity. Resistance data show a relatively stable response below ~ 500 kHz. On the other hand, capacitance measurements are constant between 100 kHz and 2 MHz only for low ionic concentration fluids; electrode polarization effects determine the measured capacitance at lower frequencies and high ionic concentrations (Klein and Santamarina 1995). Therefore resistance measurements can be reliably performed between 10 and 1000 kHz whereas capacitance measurements should be limited to the neighborhood of 500 kHz and only for low conductivity soils.

Probe Calibration: Soil Parameters

The needle probe is designed to assess the spatial variability in soil specimens by measuring the local electromagnetic properties of the soil at the tip. The electromagnetic properties are computed from the measured resistance R and reactance X , or the impedance $|Z|$ magnitude and phase angle θ . These parameters are related as follows:

$$Z^* = R + j \cdot X = |Z| \cos \theta + j \cdot |Z| \sin \theta \quad (4)$$

The pairs $R-X$ or $|Z|-\theta$ are determined with a Hewlett Packard HP-4192A low frequency impedance analyzer. The measured parameters combine the impedance of the probe, the cable, electrode effects, and the soil itself. The goal of calibration is to extract the impedance of the soil Z_{soil}^* from the measured impedance Z_{meas}^* (details are given by Cho 2001).

Calibration

Stray values are modeled as series and parallel impedances, Z_{ser}^* and Z_{par}^* [Figs. 4(a and b)]. Therefore the measured impedance

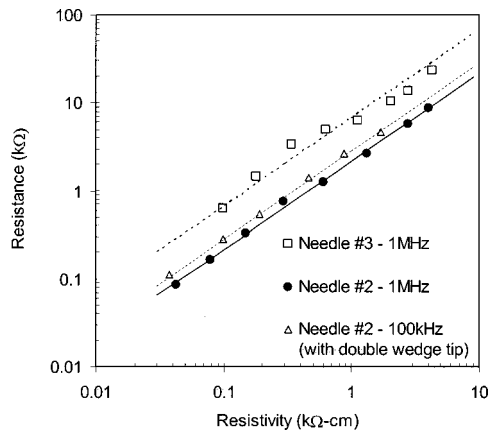


Fig. 5. Typical calibration data. Resistance measured with different needle probes versus the known resistivity of electrolytes prepared with different NaCl concentrations (voltage=1 V). Note: Stable R values are measured for a wide range of frequencies in Fig. 3.

Z_{meas}^* is

$$Z_{meas}^* = Z_{ser}^* + \frac{1}{1/Z_{par}^* + 1/Z_{soil}^*} \quad (5)$$

The unwanted series and parallel impedances, Z_{ser}^* and Z_{par}^* are obtained from two separate measurements. First, the core and the outer conductor that make up the needle are short-circuited at the tip so that Z_{par}^* is essentially removed from the circuit; in this case, the measured impedance is $(Z_{meas}^*)_{short} = Z_{ser}^*$. Then, a second measurement is conducted in “open,” where the tip of the probe is kept in air, so that the measured impedance becomes $(Z_{meas}^*)_{open} = Z_{ser}^* + Z_{par}^* = (Z_{meas}^*)_{short} + Z_{par}^*$. Finally, the known values of Z_{ser}^* and Z_{par}^* are removed from soil impedance Z_{meas}^* in Eq. (5), and the impedance of soil Z_{soil}^* for the given frequency becomes

$$Z_{soil}^* = \{[(Z_{meas}^*)_{open} - (Z_{meas}^*)_{short}]^{-1} - [(Z_{meas}^*)_{short}]^{-1}\}^{-1} \quad (6)$$

When spectral measurements are conducted $(Z_{meas}^*)_{short}$, $(Z_{meas}^*)_{open}$, Z_{meas}^* , and Z_{soil}^* are determined at each frequency.

Soil Parameters

The electrical response of a soil is modeled as a “lossy dielectric,” which involves resistor R and capacitor C in parallel,

$$Z_{soil}^* = \left[\frac{1}{R_{soil}} + j\omega C_{soil} \right]^{-1} \quad (7)$$

where $R_{soil}(\Omega)$ and $C_{soil}(F)$ =resistance and capacitance of the soil, respectively. The soil parameters, resistivity ρ_{soil} and permittivity κ'_{soil} , are related to R_{soil} and C_{soil} through geometric considerations,

$$R_{soil} = \alpha \cdot \rho_{soil} \quad (8)$$

and

$$C_{soil} = \beta \cdot \epsilon_0 \cdot \kappa'_{soil} \quad (9)$$

where factors α and β =electrode shape factors for resistance and capacitance determined by calibrating with known fluids. Fig. 5 shows the relation between resistance and resistivity for different fluids. The resistance shape factor is $\alpha=2.15 \text{ cm}^{-1}$ for needle No.

2, $\alpha=2.8 \text{ cm}^{-1}$ for a double-wedge tip, and $\alpha=6.7 \text{ cm}^{-1}$ for needle No. 3. The value of β determined with deionized water for needle No. 2 is $\beta=0.48 \text{ cm}$.

Porosity $n=V_w/V_t$ is inferred from either ρ_{soil} or κ'_{soil} (a review of related expressions can be found in work by Parkhomenko 1967 and Santamarina et al. 2001). In its simplest form, the permittivity of soils κ'_{soil} can be expressed as a volumetric average (electrical field parallel to mineral–water “layers”); if the soil is saturated,

$$\kappa'_{soil} = n \cdot \kappa'_w + (1-n) \cdot \kappa'_s \quad (10)$$

where $\kappa'_w \approx 79$ =permittivity of water; and $\kappa'_s = 3-7$ =permittivity of the mineral that makes the soil particles. From Eq. (10), the porosity n is

$$n = \frac{e}{1+e} = \frac{\kappa'_{soil} - \kappa'_s}{\kappa'_w - \kappa'_s} \quad (11)$$

The resistivity ρ_{soil} is related to the pore fluid resistivity ρ_{el} and the porosity n . According to Archie (1942),

$$\rho_{soil} = \rho_{el} \cdot n^\theta \quad (12)$$

where $\theta \approx -1$ to -2.4 ; ρ_{soil}/ρ_{el} is known as the “formation factor.” Together, permittivity and resistivity data can be used to determine not only the porosity but the pore fluid characteristics as well [Eqs. (11) and (12)].

Simplified Calibration and Measurement

The fairly constant frequency response exhibited by resistance measurements (Fig. 3) and the resistive nature of soil impedance at low frequencies suggest a simplified implementation based on resistance only, $V=R \cdot i$. This requires the determination of current i (ammeter) and drop in voltage ΔV (voltmeter). A rudimentary setup is shown in Fig. 4(c). It consists of a signal generator and a two-channel oscilloscope or analog/digital (A/D) board, as shown in Fig. 4(c) (caution: the oscilloscope channels and the signal generator may share ground). The current through the system $i=(V_S - \Delta V_N)/R_{fix}$ is determined by measuring the voltage at the source V_S and the drop in voltage across the needle ΔV_N ; therefore, the voltage drops $V_S - \Delta V_N$ across the known resistor R_{fix} . Then, soil resistance R_{soil} at the tip of the needle probe is

$$R_{soil} = \frac{\Delta V_N}{i} = \frac{\Delta V_N}{V_S - \Delta V_N} R_{fix} \quad (13)$$

The resistivity of soil ρ_{soil} can be directly related to measured R_{soil} by calibrating with fluids of known resistivity, as shown in Fig. 5. The resulting calibration parameters embody all factors, including tip shape and losses in the peripheral circuit elements.

Applications: Spatial Variability Assessment

The capability of electrical needle probes to resolve interfaces and spatial variability is now explored using undisturbed clay specimens and sand specimens prepared by different techniques. In all these cases, the needle is inserted at 1 cm/min using a screw-mount support. Much faster insertion rates can be implemented with the simplified measurement procedure since it can effectively accommodate $\sim 10^5$ measurements per second (presuming the signal applied is a 100 kHz sinusoid).

Interface Detection: Resolution

The needle probe is gradually advanced across a sharp interface to assess its resolution capability. Two cases are tested: air/

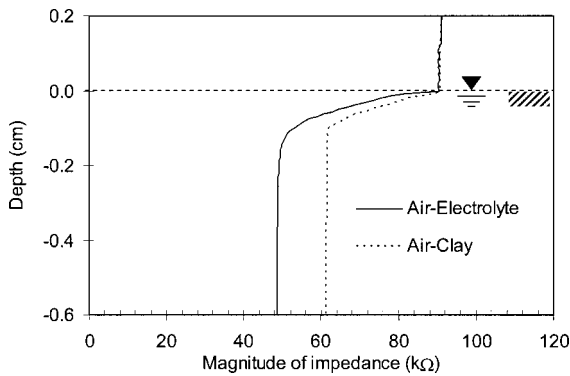


Fig. 6. Interface resolution. Two cases are shown for air–electrolyte interface and air–clay interface ($f=100$ kHz, voltage=1 V, needle No. 1). Insertion of the needle renders convolution of the step-like interface according to the shape of the needle tip.

electrolyte and air/clay. The electrolyte is a 0.001 M NaCl solution and the clay is kaolinite paste with water content $w=66\%$ (the liquid limit). The impedance is measured every 0.063 mm at $f=100$ kHz frequency. Fig. 6 shows the variation of impedance across the interface determined with needle No. 1. The length of the transition region is about the exposed length of the inner conductor along the wedge (~ 1 mm in this case); the double-hump response (the first hump is weak) reflects the interface seen by the geometry of the tip.

Two observations follow from the results shown in Fig. 6. First, the sampling interval Δz during insertion can be reduced to about half the exposed length of the inner conductor. Second, the insertion of the probe is a “convolution.” The smoothing transfer function H can be inferred from the step response (Fig. 6). Then,

measured electrical profiles can be “deconvolved” with the inverse of transfer function H^{-1} to obtain sharper, true field profiles.

Layer Detection: Clayey Soils

The unique capability of the electrical needle to detect interfaces is utilized here to explore varved clay (Connecticut Valley, $n=0.64$, LL=51, PL=31, $w=42-73\%$; de Groot and Lutenegeer 2002; see also DeJong et al. 2003). Resistance is measured every 0.254 mm at $f=100$ kHz with needle No. 2 with the double-wedge tip and a constant shaft diameter. After electromagnetic measurements, the specimen is carefully cut, photographed, and x rayed. Images and resistance profiles are shown in Fig. 7. The measured resistance profiles closely match the variability observed in the images. Clearly the electrical needle probe can be effectively used to capture the spatial variability of varved clays and to determine characteristic internal length scales in soils.

The resistance profile for undisturbed Mexico City soil specimens was determined and is shown in Fig. 8 ($n=0.91$, LL=338, PL=80, $w\approx 240\%$; Díaz-Rodríguez 2002). Compared to the Connecticut Valley varved clay, Mexico City soil appears to be a very uniform, homogeneous deposit (note the differences in scale between Figs. 7 and 8).

Needle Size and Internal Scales

The large and small probes (needles Nos. 2 and 3) are gradually inserted into 10 specimens prepared with different grain sizes by the water pluviation method to attain the most homogeneous soils possible (tap water, $\rho_{el}=23$ kΩ cm). The complex permittivity is measured every 0.5 mm at $f=100$ kHz. Spatial variation of the resistance for two specimens are shown in Fig. 9. Fig. 10 shows

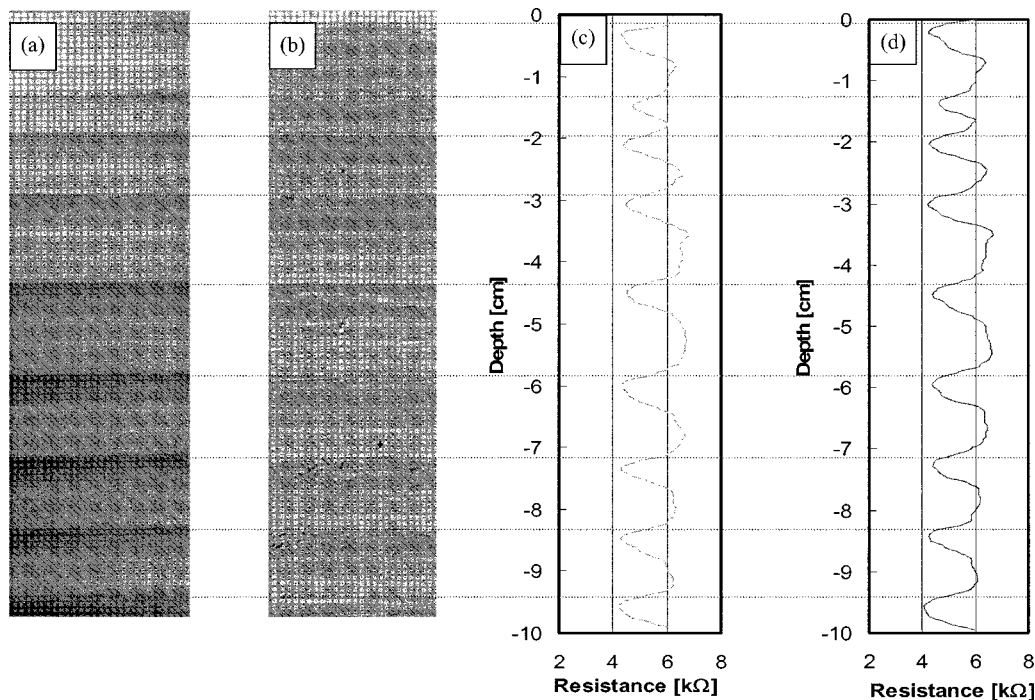


Fig. 7. Detection of layering in Connecticut Valley varved clay: (a) X-ray image; (b) photograph; and (c), (d) measured resistance versus depth at two different locations 7 cm apart ($f=100$ kHz, voltage=1 V, needle No. 2 with double-wedge tip). The resistance measured for pore fluid $R_{el}=3.17$ kΩ.

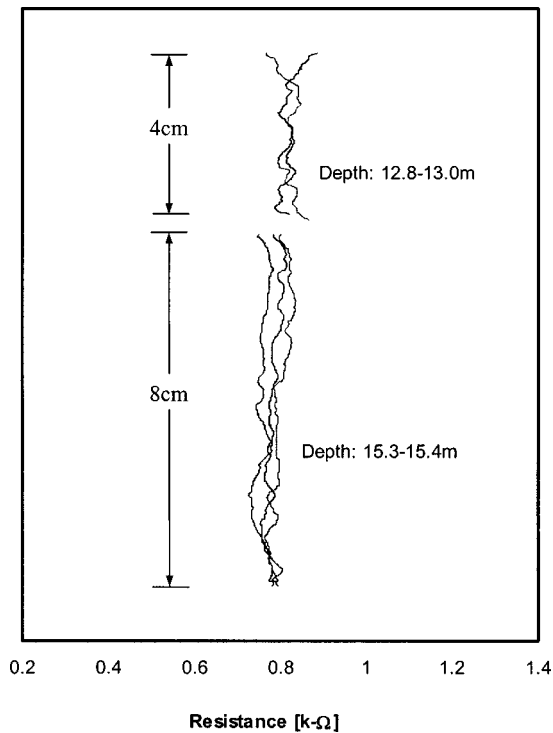


Fig. 8. Spatial variability in Mexico City soil specimens ($f = 100$ kHz, voltage=1 V, needle No. 2 with double-wedge tip). For comparison, the amplitude of resistance oscillations detected in varved clays is 2 k Ω (cf. Fig. 7). Resistance measured for pore fluid $R_{el} = 0.34$ k Ω .

the computed coefficient of variation (COV) (standard deviation/mean) for each of the 20 soil profiles versus the ratio d_{probe}/D_{50} between the size of the probe d_{probe} and the mean size of soil particles D_{50} . The coefficient of variation increases as the size of probe d_{probe} and associated sampling interval Δz comes close to the size of the particle (this is the limit of spatial aliasing for the grain length scale). On the other hand, a very large d_{probe}/D_{50} ratio prevents the detection of pore-size soil variations due to

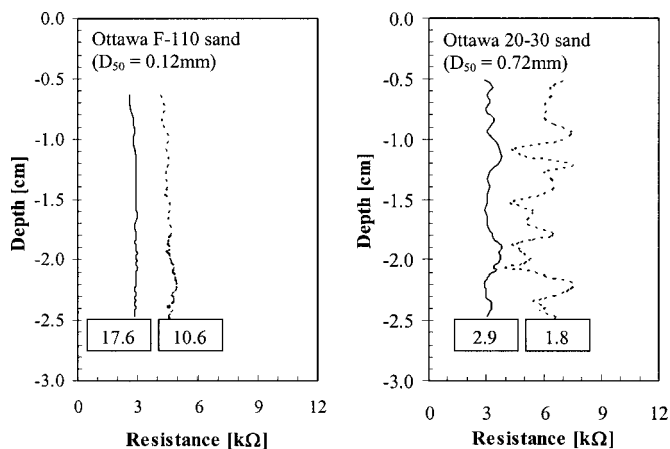


Fig. 9. Tip size versus internal length scale. Two sands of different grain size are tested with a large and a small needle: needle No. 2 (solid line); and needle No. 3 (dotted line). The ratios d_{probe}/D_{50} are indicated in the square blocks ($f = 100$ kHz; voltage=1 V).

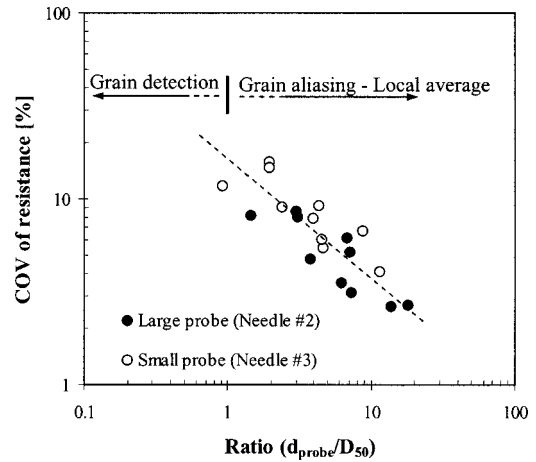


Fig. 10. Needle size to particle size d_{probe}/D_{50} effects ($f = 100$ kHz; voltage=1 V); and detection of spatial variability

averaging effects (this is equivalent to a moving average kernel). Thus, the probe size can be selected to capture different scales of interest.

Specimen Preparation Effects

Ottawa F-110 sand ($D_{50} = 0.12$ mm, $e_{max} = 0.848$, $e_{min} = 0.535$) is used to explore specimen preparation effects. Three specimens are prepared by air pluviation, moist tamping, and water pluviation procedures. The complex impedance Z^* is measured every 0.5 mm, corrected for stray parameters [Eq. (7)], and converted into permittivity. The void ratios estimated from the permittivity [Eq. (11)] are shown in Fig. 11; the apparent resolvability is $\Delta e \approx 0.01$. It is observed that the specimen prepared by the moist tamping method has the highest variation in void ratio, while the specimen prepared by water pluviation shows the lowest variation (in agreement with observations by Jang et al. (1999) who used impregnation and image analysis techniques).

Conclusions

Routine assessment of spatial variability in soil specimens facilitates interpretation of the observed soil response. A new labora-

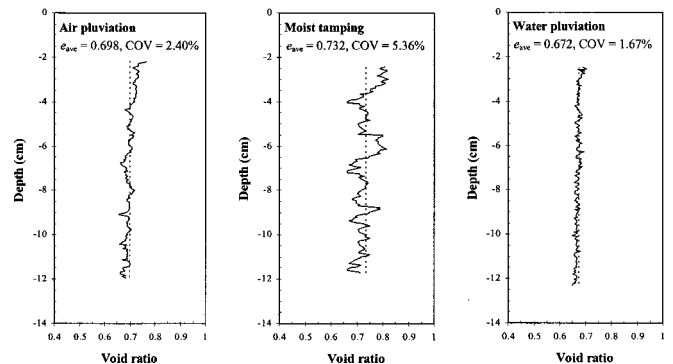


Fig. 11. Variability of void ratio for three different specimen preparation methods (Ottawa F-110 sand: $D_{50} = 0.12$ mm, $e_{max} = 0.848$, $e_{min} = 0.535$). Local void ratio is determined from κ' measurements ($f = 1$ MHz, voltage=1 V, needle No. 2). e_{ave} is the global void ratio of the specimen and COV is the coefficient of variation.

tory device was developed for effective one-dimensional assessment of spatial variability in clays and sands. It is based on local measurements of complex impedance to assess the spatial variability of either the porosity or fluid resistivity, or both. The operating frequency should be selected by taking into consideration electrode polarization, corrosion, equipment resonance, and the spectral response of the soil. Stable resistance measurements can be conducted using readily available electronic devices in a wide frequency range. The size of the needle probe can be selected according to the scale of interest. Probes that are ~ 2 mm in diameter permit millimetric resolution of interfaces and variability, and are sensitive to relatively small local variations of the void ratio ($\Delta e \approx 0.01$).

Acknowledgments

This study was supported by the National Science Foundation (research on scales in soils), the Mid-America Earthquake Center, and the NSF-NEES Project (University of California at Davis, directed by B. L. Kutter). D. J. DeGroot provided the varved clay specimen and J. A. Díaz-Rodríguez provided the Mexico City soil sample.

References

Archie, G. E. (1942). "The electrical resistivity log as an aid in determining some reservoir characteristics." *Trans. Am. Inst. Min., Metall. Pet. Eng.*, 146, 54–62.

Baligh, M. M., and Scott, R. F. (1976). "Quasi-static deep penetration in clay." *J. Geotech. Eng. Div., Am. Soc. Civ. Eng.*, 101(11), 1119–1133.

Bradford, S. A. (1993). *Corrosion control*, Van Nostrand Reinhold, New York.

Cho, G. C. (2001). "Unsaturated soil stiffness and postliquefaction shear strength." PhD thesis, Georgia Inst. of Technology, Atlanta.

Davidson, J. L., and Boghrat, A. (1983). "Displacement and strains around probes in sand." *Proc., Conf. on Geotech. Practice in Offshore Engineering*, S. G. Wright, ed., Univ. of Texas at Austin, Austin, Tex., 181–202.

DeGregorio, V. B. (1990). "Loading systems, sample penetration, and liquefaction." *J. Geotech. Eng.*, 116(5), 805–821.

DeGroot, D. J., and Lutenecker, A. J. (2002). "Geology and engineering properties of Connecticut Valley varved clay." *Characterisation and Engineering Properties of Natural Soils*, T. S. Tan, K. K. Phoon, D. W. Hight, and S. Leroueil, eds., 693–724.

De Jong, J. T., DeGroot, D. J., Yafate, N. J., and Jakubowski, J. (2003). "Detection of soil layering using a miniature piezoprobe." *12th Pan-American Conf. on Soil Mechanics and Geotechnical Engineering*, P. J. Culligan, H. H. Eistein, and A. J. Whittle, eds., 151–156.

Desrues, J., Chambon, R., Mokni, M., and Mazerolle, F. (1996). "Void ratio evolution inside shear bands in triaxial sand specimens studied by computed tomography." *Geotechnique*, 46(3), 529–546.

Díaz-Rodríguez, J. A. (2002). "Characterization and engineering properties of Mexico City lacustrine soils." *Characterisation and engineering properties of natural soils*, T. S. Tan, K. K. Phoon, D. W. Hight, and S. Leroueil, eds., 725–755.

Fenton, G. A., and Griffiths, D. V. (1996). "Statistics of free surface flow through stochastic earth dam." *J. Geotech. Eng.*, 122(6), 427–436.

Griffiths, D. V., and Fenton, G. A. (1993). "Seepage beneath water retaining structures founded on spatially random soil." *Geotechnique*, 43(4), 577–587.

Ishihara, K. (1993). "Liquefaction and flow failure during earthquakes." *Geotechnique*, 43(3), 351–415.

Jang, D. J., Frost, J. D., and Park, J. Y. (1999). "Preparation of epoxy impregnated sand coupons for image analysis." *Geotech. Test. J.*, 22(2), 147–158.

Klein, K., and Santamarina, J. C. (1995). "Polarization and conduction of clay-water-electrolyte systems." *J. Geotech. Eng.*, 121(3), 243–248.

Kokusho, T. (1999). "Water film in liquefied sand and its effect on lateral spread." *J. Geotech. Geoenviron. Eng.*, 125(10), 817–826.

Ladd, R. S. (1977). "Specimen preparation and cyclic stability of sands." *J. Geotech. Eng. Div., Am. Soc. Civ. Eng.*, 103(6), 535–547.

Lee, J. S. (2003). "High resolution geophysical techniques for small-scale soil model testing." PhD thesis, Georgia Inst. of Technology, Atlanta.

Marcuson, III, W. F., Hynes, M. E., and Fanklin, A. G. (1990). "Evaluation and use of residual strength in seismic safety analysis of embankments." *Earthquake Spectra*, 6(3), 529–572.

Mitchell, J. K., Chatoian, J. M., and Carpenter, G. C. (1976). "The influences of sand fabric on liquefaction behavior." *Rep. No. TE 76-1*, U.S. Army Engineer Waterways Experiment Station, Univ. of California, at Berkeley, Berkeley, Calif.

Miura, S., and Toki, S. (1982). "A sample preparation method and its effect on static and cyclic deformation-strength properties of sand." *Soils Found.*, 22(1), 61–77.

Mulilis, J. P., Chan, C. K., and Seed, H. B. (1975). "The effects of method of sample preparation on the cyclic stress strain behavior of sands." *EERC Rep. No. 75-18*, Environmental Engineering Research Council.

Mulilis, J. P., Seed, H. B., Chan, C. K., Mitchell, J. K., and Arulanandan, K. (1977). "Effects of sample preparation on sand liquefaction." *J. Geotech. Eng. Div., Am. Soc. Civ. Eng.*, 103(2), 91–108.

Paice, G. M., Griffiths, D. V., and Fenton, G. A. (1996). "Finite element modeling of settlements on spatially random soil." *J. Geotech. Eng.*, 122(9), 777–779.

Parkhomenko, E. I. (1967). *Electrical properties of rocks*, Plenum, New York.

Phoon, K. K., and Kulhawy, F. H. (1999). "Characterization of geotechnical variability." *Can. Geotech. J.*, 36(4), 612–624.

Popescu, R., and Prevost, J. H. (1996). "Influence of spatial variability of soil properties on seismically induced soil liquefaction." *Geotechnical Spec. Publ. No. 58*, 1098–1112.

Popescu, R., Prevost, J. H., and Deodatis, G. (1997). "Effects of spatial variability on soil liquefaction: some design recommendations." *Geotechnique*, 47(5), 1019–1036.

Santamarina, J. C. in collaboration with Klein, K. A., and Fam, M. A. (2001). *Soils and waves—Particulate materials behavior, characterization and process monitoring*, Wiley, New York.

Tonon, F., Bernardini, A., and Mammino, A. (2000). "Reliability analysis of rock mass response by means of random set theory." *Reliability Eng. Sys. Safety*, 70(3), 263–282.

Townsend, F. C. (1978). "A review of factors affecting cyclic triaxial tests." *Dynamic Geotech. Testing*, ASTM STP 654, 356–383.

Vasquez-Herrera, A., and Dobry, R. (1988). "Pore pressure buildup and liquefaction failure of anisotropically consolidated sand due to cyclic straining." *Geotechnical Spec. Publ. No. 21*, 346–366.

Vesic, A. S. (1977). "Design of pile foundations, National Cooperative Highway Research Program, synthesis of highway proactive 42." Transportation Research Board, Washington, D.C., 12–22.

Yong, R. N., Alonso, E., and Tappa, M. M. (1977). "Application of risk analysis to the prediction of slope stability." *Can. Geotech. J.*, 14(4), 540–553.